Role of Solvent Dynamics in Ultrafast Photoinduced Proton−Coupled Electron Transfer Reactions in Solution

ARTICLE *in* THE JOURNAL OF PHYSICAL CHEMISTRY B · SEPTEMBER 2010

Impact Factor: 3.3 · DOI: 10.1021/jp1051547 · Source: PubMed

3 AUTHORS, INCLUDING:

Alexander V. Soudackov
University of Illinois, Urbana-Champaign
54 PUBLICATIONS **1,729** CITATIONS

Role of Solvent Dynamics in Ultrafast Photoinduced Proton-Coupled Electron Transfer Reactions in Solution

Anirban Hazra, Alexander V. Soudackov, and Sharon Hammes-Schiffer*

Department of Chemistry, Pennsylvania State University, University Park, Pennsylvania 16802

Received: June 4, 2010; Revised Manuscript Received: July 29, 2010

A theoretical formulation for modeling photoinduced nonequilibrium proton-coupled electron transfer (PCET) reactions in solution is presented. In this formulation, the PCET system is described by donor and acceptor electron−proton vibronic free energy surfaces that depend on a single collective solvent coordinate. Dielectric continuum theory is used to obtain a generalized Langevin equation of motion for this collective solvent coordinate. The terms in this equation depend on the solvent properties, such as the dielectric constants, relaxation time, and molecular moment of inertia, as well as the solute properties characterizing the vibronic surfaces. The ultrafast dynamics following photoexcitation is simulated using a surface hopping method in conjunction with the Langevin equation of motion. This methodology is used to examine a series of model photoinduced PCET systems, where the initial nonequilibrium state is prepared by vertical photoexcitation from the ground electronic state to the donor electronic state. Analysis of the dynamical trajectories provides insight into the interplay between the solvent dynamics and the electron−proton transfer for these types of processes. In addition, these model studies illustrate how the coupling between the electron−proton transfer and the solvent dynamics can be tuned by altering the solute and solvent properties.

I. Introduction

Photoinduced proton-coupled electron transfer (PCET) reactions are important in a broad range of energy conversion devices, such as solar cells, as well as in both natural and artificial photosynthesis.[1−8] The investigation of these reactions in chemical model systems has provided insight into the fundamental principles governing such processes.[9−14] A significant challenge has been to determine the relative time scales of the solvent, electron, and proton motions, as well as the degree of coupling among them. In addition, the role of solvent dynamics, which has been studied extensively for electron transfer reactions,[15] is not yet well understood for photoinduced PCET processes. The present paper focuses on concerted PCET reactions, where the electron and proton transfer in a single step without a stable intermediate.[16−19] Recently, several chemical model systems exhibiting photoinduced concerted PCET have been studied experimentally with a variety of spectroscopic methods that can probe a wide range of time scales, including the ultrafast dynamics in some cases.[9−14]

One type of chemical system that has been studied experimentally is photoinduced PCET in charge transfer excited states of hydrogen-bonded organic molecules. A specific example is photoinduced PCET in the hydrogen-bonded adduct of *p*-nitrophenylphenol, denoted O_2N−OH for simplicity, and *tert*-butylamine, denoted NH_2-*t*-Bu. A proposed PCET pathway for this process is as follows[14]

$$O_2N{-}OH\cdots H_2N\text{-}t\text{-}Bu \xrightarrow{h\nu} {}^{-\bullet}O_2N{-}{}^{+\bullet}OH\cdots H_2N\text{-}t\text{-}Bu \xrightarrow{\text{EPT}} O_2N{-}O^{-}\cdots {}^{+}H_3N\text{-}t\text{-}Bu \quad (1)$$

The electronic ground state is on the left, the photoexcited donor state is in the middle, and the acceptor state is on the right. In this process, photoexcitation leads to the transfer of an electron within the *p*-nitrophenylphenol, from an orbital localized on the OH group to an orbital localized on the O_2N group. Subsequently, a concerted electron−proton transfer (EPT) reaction occurs, in which the electron transfers back (within the *p*-nitrophenylphenol molecule) and the proton transfers from the OH group of *p*-nitrophenylphenol to the NH_2 group of *tert*-butylamine. Another possible mechanism is that, after the initial photoexcitation, the proton transfers from the OH group to the NH_2 group, followed by an EPT recombination step back to the ground state. More complex mechanisms are also possible. In addition, other pathways involving singlet−triplet conversion are thought to occur in the overall process.[14]

Another type of photoinduced PCET system that has been studied experimentally is the quenching of metal-to-ligand charge transfer (MLCT) states in transition metal complexes. A specific example is photoinduced PCET associated with the quenching of a MLCT excited state of the ruthenium complex $Ru(bpy)_2(bpz)$, where bpy denotes 2,2′-bipyridine and bpz denotes 2,2′-bipyrazine, by hydroquinone, denoted H_2Q. A proposed PCET mechanism for this process is as follows[13,14]

$$(bpy)_2Ru^{II}(bpz)^{2+} + H_2Q \xrightarrow{h\nu} (bpy)_2Ru^{III}(bpz^{-\bullet})^{2+} + H_2Q \xrightarrow{\text{EPT}} (bpy)_2Ru^{II}(bpzH^{\bullet})^{2+} + {}^{\bullet}HQ \quad (2)$$

Again, the electronic ground state is on the left, the photoexcited donor state is in the middle, and the acceptor state is on the right. In this process, photoexcitation leads to the transfer of an electron from the Ru to the bpz ligand. Subsequently, an EPT reaction occurs in which an electron transfers from H_2Q to the Ru and a proton transfers from H_2Q to the nitrogen atom of the bpz ligand. Analysis of the kinetics is complicated by the formation of the hydrogen-bonded complex, which may occur after the photoexcitation.[14]

* To whom correspondence should be addressed. E-mail: shs@chem.psu.edu.

10.1021/jp1051547
Published on Web 09/01/2010

Although these two reactions are quite different, they share two common features. In both cases, the electronic ground state and the acceptor state (i.e., the left and right sides of the above equations) have similar charge distributions, while the photoexcited donor state (the middle species) has a distinctly different charge distribution because of electron transfer within either the *p*-nitrophenylphenol or the ruthenium complex. Thus, the equilibrium solvent configuration will be similar for the electronic ground state and the acceptor state but will be distinctly different for the photoexcited donor state. Moreover, in both cases, the proton is not transferred immediately upon photoexcitation but rather transfers with the electron in the concerted EPT step. Thus, the proton potential is similar for the electronic ground state and the photoexcited donor state (i.e., the proton is bonded to the same atom), while the proton potential is distinctly different for the acceptor state (i.e., the proton is bonded to a different atom). Note that the proton potential could be somewhat perturbed due to stretching of the O−H bond in the photoexcited donor state.

The objective of this paper is to develop a theoretical formalism to describe the ultrafast dynamics of these types of photoinduced PCET processes. Most previous theoretical studies of PCET processes have focused on thermally activated reactions using analytical theories[16,19−24] related to Marcus theory for electron transfer.[25,26] In these studies, the transferring proton was treated quantum mechanically, and the solvent was either represented by a dielectric continuum model[27−33] or treated by molecular dynamics simulations with explicit solvent molecules.[34−36] In contrast to thermally activated reactions, however, photoinduced reactions are typically associated with highly nonequilibrium initial conditions. The nonadiabatic dynamics of both thermally activated and photoinduced PCET reactions have been studied using surface hopping methods[37,38] for simple model systems including only a single effective solvent coordinate without dissipative effects.[39−41] More recently, photoinduced PCET reactions have been studied using a model Hamiltonian based on a two-state system coupled to a harmonic bath, in conjunction with a golden rule formulation invoking the assumption that the solvent remains in equilibrium throughout the EPT process.[42,43]

The assumption that the solvent remains at equilibrium is reasonable for thermally activated reactions and for photoinduced reactions in which the time scale of the solvent dynamics is much faster than the time scale of the EPT process. This assumption breaks down, however, when the solvent dynamics and EPT occur on similar time scales. One possible approach for studying these types of photoinduced PCET processes is to perform nonadiabatic molecular dynamics simulations with explicit solvent molecules using either an ab initio or an empirical valence bond[44,45] potential, in conjunction with a quantum mechanical treatment of the transferring proton. Such simulations are computationally expensive, however, and comparison to ultrafast experimental data relies on the use of highly accurate potential energy surfaces for the description of both the charge transfer process and the solvent dynamics.

In the present paper, we adopt an alternative strategy, in which the solvent environment is represented as a dielectric continuum, and dissipative effects are included via stochastic Langevin dynamics. In particular, we use dielectric continuum theory to obtain a generalized Langevin equation of motion for a collective solvent coordinate. The terms in this equation are defined in terms of the frequency-dependent dielectric function characterizing the dielectric properties of the solvent and depend on the solvent dielectric constants, relaxation time scale, and molecular moment of inertia. The PCET reaction is described in terms of quantum transitions between donor and acceptor electron−proton vibronic states obtained from a model Hamiltonian. The electron−proton vibronic free energy surfaces depend on the collective solvent coordinate, and the nonadiabatic dynamics on these surfaces is simulated using a surface hopping method in conjunction with the Langevin equation of motion. Analysis of the dynamical trajectories provides insight into the interplay between the solvent dynamics and the EPT. In contrast to explicit molecular dynamics simulations, this approach is computationally efficient and utilizes experimentally measured macroscopic solvent properties.

The remainder of the paper is organized as follows. Section II presents the theoretical formulation, specifying the model Hamiltonian, the adiabatic vibronic free energy surfaces, the Langevin equation of motion for the collective solvent coordinate, and the surface hopping dynamics on the adiabatic vibronic free energy surfaces. Section III describes the model systems and the simulation details, followed by the analysis of the results and a discussion of the limitations of the models. Concluding remarks and future directions are discussed in section IV.

II. Theory

A. Model Hamiltonian for a PCET Reaction Complex. Our model for a photoinduced PCET reaction is based on a two-state description of the electronic subspace spanned by two diabatic electronic states $|\mathrm{D}\rangle$ and $|\mathrm{A}\rangle$ corresponding to an electron localized on the electron donor and acceptor sites, respectively. The proton is described by a single coordinate r_p spanning the range between the proton donor and acceptor sites. For simplicity, we neglect the remaining degrees of freedom describing the intramolecular vibrations within the reaction complex, assuming that these vibrations are uncoupled from the motions relevant to the PCET reaction. Two distinct proton potentials $U^\mathrm{D}(r_\mathrm{p})$ and $U^\mathrm{A}(r_\mathrm{p})$, corresponding to the diabatic electronic states $|\mathrm{D}\rangle$ and $|\mathrm{A}\rangle$, are assumed to have minima near the proton donor and acceptor sites, respectively.

With these assumptions, the gas phase electronic Hamiltonian for the model PCET reaction complex can be represented as the following 2×2 matrix in the basis of the diabatic electronic states $|\mathrm{D}\rangle$ and $|\mathrm{A}\rangle$

$$H_0^\mathrm{el} = \begin{bmatrix} U^\mathrm{D}(r_\mathrm{p}) & V_\mathrm{DA} \\ V_\mathrm{DA} & U^\mathrm{A}(r_\mathrm{p}) - \Delta \end{bmatrix} \tag{3}$$

where V_DA is the electronic coupling, which is assumed to be a real constant, and Δ is the electronic energy bias parameter. The total gas phase Hamiltonian for the reaction complex is then obtained by including the kinetic energy of the proton

$$H_0 = T_\mathrm{p} + H_0^\mathrm{el} \tag{4}$$

where $T_\mathrm{p} = -(\hbar^2/2m_\mathrm{p})\partial^2/\partial r_\mathrm{p}^2$ is the proton kinetic energy operator and m_p is the mass of the proton.

B. Adiabatic Vibronic Free Energy Surfaces. The interaction with the solvent degrees of freedom is introduced within the framework of dielectric continuum theory.[27−33] Consider a PCET system with a reaction complex (solute) described by the gas phase Hamiltonian H_0 and immersed in a uniform and isotropic dielectric medium characterized by the scalar frequency-dependent dielectric function $\varepsilon(\omega)$. For this system, the solvent degrees of freedom are represented by an inertial polarization

vector field $\mathbf{P}(\mathbf{r})$ depending on the spatial coordinate $\mathbf{r}$. Within this model, the solute−solvent interaction matrix elements in the basis of the two diabatic electronic states are functionals of the polarization field and are represented by the following volume integrals

$$V_{ij}^{S}[\mathbf{P}] = \iint \mathrm{d}v\,\mathrm{d}v' \frac{\rho_{ij}(\mathbf{r})\mathbf{P}(\mathbf{r}')\cdot(\mathbf{r}-\mathbf{r}')}{|\mathbf{r}-\mathbf{r}'|^3} = -\int \mathrm{d}v\,\mathbf{P}(\mathbf{r})\cdot\mathbf{D}_{ij}(\mathbf{r}) \qquad i,j = \mathrm{D},\mathrm{A} \quad (5)$$

where $\rho_{ij}(\mathbf{r})$ are the matrix elements of the total charge density operator for the reaction complex and $\mathbf{D}_{ij}(\mathbf{r})$ are the corresponding vacuum electric fields (or electric displacement fields). In the following, we will assume that the total charge densities do not depend on the proton coordinate r_p and that the off-diagonal densities $\rho_{DA}(\mathbf{r})$ vanish. These assumptions are reasonable because the range of the proton motion (∼1 Å) is small compared to the size of the reaction complex, and the diabatic electronic states are highly localized by construction.

In this framework, the matrix elements of the total electron−proton Hamiltonian are functionals of the inertial polarization field $\mathbf{P}(\mathbf{r})$. Moreover, the adiabatic vibronic free energy functionals $\mathscr{U}_k[\mathbf{P}]$ corresponding to the electron−proton adiabatic vibronic states can be represented as the eigenvalues of a surrogate vibronic Hamiltonian constructed in an appropriate basis of direct products of the proton vibrational states and the two diabatic electronic states. This surrogate vibronic Hamiltonian is of the form

$$\tilde{H}[\mathbf{P}] = \frac{1}{2}f_0\int \mathrm{d}v\,\mathbf{P}^2(\mathbf{r}) + T_p + \begin{bmatrix} U^{D}(r_p) + V_{DD}^{S}[\mathbf{P}] & V_{DA} \\ V_{DA} & U^{A}(r_p) + V_{AA}^{S}[\mathbf{P}] - \Delta \end{bmatrix} \quad (6)$$

where the first term describes the polarization field self free energy and $f_0 = 4\pi\varepsilon_0\varepsilon_\infty/(\varepsilon_0 - \varepsilon_\infty)$ is the inverse Pekar factor.

C. Langevin Equation of Motion for Collective Solvent Coordinate. The adiabatic vibronic free energy functionals $\mathscr{U}_k[\mathbf{P}]$ defined via the surrogate Hamiltonian given in eq 6 provide the basis for the derivation of the equations of motion for the time-dependent inertial polarization field $\mathbf{P}(\mathbf{r},t)$. The standard procedure starting from the Maxwell equations for the properly coarse-grained dielectric continuum medium leads to the following generalized Langevin equation describing the time evolution of the inertial polarization field $\mathbf{P}(\mathbf{r},t)$ for the kth adiabatic vibronic free energy functional $\mathscr{U}_k[\mathbf{P}]$[28,46−48]

$$(\hat{f} - f_0)\mathbf{P}(\mathbf{r},t) = -\frac{\delta\,\mathscr{U}_k[\mathbf{P}]}{\delta\mathbf{P}} + \mathbf{F}(\mathbf{r},t) \quad (7)$$

where $\mathbf{F}(\mathbf{r},t)$ is the random field describing thermal fluctuations of the polarization.[46] Here, $\hat{f}$ is a causal integral operator defined via its action on an arbitrary time-dependent function $g(t)$

$$\hat{f}g(t) = \int_{-\infty}^{t} f(t-\tau)g(\tau)\,\mathrm{d}\tau \quad (8)$$

The integral kernel $f(t)$ is related to the frequency-dependent factor $f(\omega) = 4\pi\varepsilon(\omega)\varepsilon_\infty/[\varepsilon(\omega) - \varepsilon_\infty]$ through the Fourier transform

$$f(t) = \frac{1}{2\pi}\int_{-\infty}^{\infty} f(\omega)\mathrm{e}^{-\mathrm{i}\omega t}\,\mathrm{d}\omega \quad (9)$$

For a model based on two electronic states, eq 7 can be recast in terms of a scalar collective solvent coordinate x[28,48]

$$(\hat{f} - f_0)x(t) = -\frac{\mathrm{d}W_k(x)}{\mathrm{d}x} + F(t) \quad (10)$$

The collective solvent coordinate x is a scaled energy gap reaction coordinate[49] defined via the following volume integral

$$x = \sqrt{\frac{f_0}{2\lambda}}\int \mathrm{d}v\,[\mathbf{P}(\mathbf{r}) - \mathbf{P}_D(\mathbf{r})][\mathbf{P}_A(\mathbf{r}) - \mathbf{P}_D(\mathbf{r})] \quad (11)$$

where $\mathbf{P}_D(\mathbf{r})$ and $\mathbf{P}_A(\mathbf{r})$ are the time-independent equilibrium polarization fields corresponding to the charge distributions in the diabatic electronic states $|D\rangle$ and $|A\rangle$, respectively. Here, λ is the solvent reorganization energy, defined as

$$\lambda = \frac{f_0}{2}\int \mathrm{d}v\,[\mathbf{P}_A(\mathbf{r}) - \mathbf{P}_D(\mathbf{r})]^2 \quad (12)$$

The random force $F(t)$ satisfies the fluctuation−dissipation theorem and is defined via its time correlation function expressed in terms of the real and imaginary parts of the generalized susceptibility $\kappa(\omega) = [f(\omega)]^{-1} = \kappa'(\omega) + \mathrm{i}\kappa''(\omega)$

$$\langle F(t)F(t')\rangle = \frac{1}{2\pi}\int_{-\infty}^{\infty}\frac{2k_BT}{\omega}\frac{\kappa''(\omega)}{|\kappa(\omega)|^2}\mathrm{e}^{-\mathrm{i}\omega(t-t')}\,\mathrm{d}\omega \quad (13)$$

The scalar function $W_k(x)$ corresponds to the kth adiabatic vibronic free energy surface, which can be obtained by diagonalization of the following surrogate vibronic Hamiltonian in an electron−proton vibronic basis

$$H^{vib} = T_p + \begin{bmatrix} U^{D}(r_p) + \frac{1}{2}f_0x^2 & V_{DA} \\ V_{DA} & U^{A}(r_p) + \frac{1}{2}f_0(x - \sqrt{2\lambda/f_0})^2 - \tilde{\Delta} \end{bmatrix} \quad (14)$$

Here, $\tilde{\Delta}$ includes the difference in solvation free energies of the two diabatic electronic states. Equation 14 indicates that the diabatic free energy surfaces along the solvent coordinate x given by the diagonal elements of H^{vib} are harmonic functions of x and thus represent the familiar Marcus theory picture of two sets of shifted intersecting parabolas.

In the Appendix, we derive the Langevin equation for the specific case of the Onodera model[50] for dielectric relaxation of the solvent. This model introduces corrections to the conventional Debye model at short times (high frequencies) to account for the inertial behavior of the polarization. In contrast to the Debye model, which describes instantaneous induced polarization, full polarization in the Onodera model can be established only after a certain short time period associated with the characteristic rotational time scale of the solvent molecules. Using the Onodera model, the generalized Langevin equation of motion in eq 10 assumes the following explicit form

$$m_x\ddot{x} = -f_0\tilde{\tau}_L\dot{x} - \frac{dW_k(x)}{dx} + F(t) \quad (15)$$

where m_x is given by eq A13 and $\tilde{\tau}_L$ is defined in eq A4. As described in the Appendix, the collective solvent coordinate is associated with an effective mass m_x that can be estimated from the microscopic parameters characterizing the individual solvent molecules (i.e., the moment of inertia).

D. Calculation of the Adiabatic Vibronic Free Energy Surfaces. In practice, the adiabatic vibronic free energy surfaces $W_k(x)$ are obtained by diagonalization of the surrogate vibronic Hamiltonian in eq 14 in an appropriate electron−proton basis. For the calculations presented in this paper, the proton basis functions are chosen to be the n_p lowest-energy eigenfunctions $\chi_\mu(r_p)$ of the following eigenvalue equation

$$[T_p + U^0(r_p)]\chi_\mu(r_p) = \epsilon_\mu^p\chi_\mu(r_p) \quad (16)$$

where $U^0(r_p) = (1/2)m_p\omega_p^2r_p^2$ is a harmonic potential centered at $r_p = 0$ with frequency ω_p.

The $2n_p$ electron−proton basis functions in the vibronic basis are represented as direct products of the two electronic diabatic states and the proton vibrational basis functions defined above. The resulting vibronic basis has the following elements

$$\{|\chi_0\rangle|D\rangle, |\chi_1\rangle|D\rangle, ...|\chi_{n_p-1}\rangle|D\rangle, |\chi_0\rangle|A\rangle, |\chi_1\rangle|A\rangle, ...|\chi_{n_p-1}\rangle|A\rangle\} \quad (17)$$

This choice of proton basis set is convenient because the basis functions are orthogonal, and the matrix elements can be evaluated analytically for proton potentials of polynomial form.[51] Note that this vibronic basis can also be used for block diagonalization of eq 14, where each block is associated with either the donor or the acceptor electronic state, $|D\rangle$ or $|A\rangle$, respectively.

E. Mixed Quantum-Classical Dynamics on the Adiabatic Vibronic Surfaces. The Langevin equation describing the dynamics of the collective solvent coordinate on a single adiabatic vibronic free energy surface $W_k(x)$ is given by eq 15. Photoinduced PCET reactions involve nondiabatic dynamics on multiple adiabatic vibronic free energy surfaces. To describe this nonadiabatic process, we use Tully's fewest switches surface hopping method,[37] also known as the molecular dynamics with quantum transitions (MDQT) method.[38] In this method, an ensemble of trajectories is propagated, and each trajectory evolves classically on a single adiabatic surface, except for instantaneous transitions among the adiabatic states. These nonadiabatic transitions are incorporated using a probabilistic algorithm designed to ensure that the fraction of trajectories in each state k at any time t is equal to the quantum probability determined from propagation of the time-dependent Schrödinger equation. Our application of the MDQT method differs from previous applications in that the classical coordinate x is propagated on mixed electron−proton vibronic surfaces $W_k(x)$ according to the stochastic Langevin equation given in eq 15.

In our implementation, the time-dependent electron−proton wave function $\Psi(t)$ is expanded in a basis of N_{ad} adiabatic electron−proton vibronic states

$$\Psi(t) = \sum_{n=1}^{N_{ad}} C_n(t)\Phi_n(x) \quad (18)$$

where the adiabatic electron−proton vibronic wave functions $\Phi_n(x)$ with energies $W_n(x)$ are obtained by diagonalization of the surrogate vibronic Hamiltonian in eq 14 in the electron−proton basis described in section II.D. The quantum amplitudes $C_n(t)$ are determined by propagating the time-dependent Schrödinger equation

$$i\hbar\dot{C}_k(t) = \sum_{n=0}^{N_{ad}} C_n(t)[W_k(x)\delta_{nk} - i\hbar\dot{x}d_{kn}(x)] \quad (19)$$

where the nonadiabatic couplings $d_{kn}(x)$ are defined as

$$d_{kn}(x) = \left\langle \Phi_k \middle| \frac{\partial\Phi_n}{\partial x} \right\rangle = \frac{\langle\Phi_k|\partial H^{vib}/\partial x|\Phi_n\rangle}{W_n(x) - W_k(x)} \quad (20)$$

These equations for the quantum amplitudes are integrated simultaneously with the Langevin equation for the solvent coordinate x given in eq 15.

In the MDQT method, the kinetic energy of the classical subsystem is adjusted to maintain energy conservation after a nonadiabatic transition.[37,38] The relation between the kinetic energy along the collective solvent coordinate and the true microscopic kinetic energy of the solvent is not trivial but can be established using the harmonic bath representation, which is formally equivalent to the dielectric continuum model within the linear response approximation.[52] Our definition of the mixed quantum-classical system, however, is based on the surrogate Hamiltonian given in eq 14 and the one-dimensional classical Langevin equation of motion given in eq 15, implying that the kinetic energy of the classical subsystem is associated only with the single collective solvent coordinate x. The corresponding effective mass m_x is defined in terms of the microscopic solvent parameters and the temperature, and the kinetic energy of the classical subsystem is $m_x\dot{x}^2/2$. In our implementation of MDQT, this definition of the kinetic energy is used to adjust the velocity $\dot{x}$ associated with the collective solvent coordinate in order to maintain total energy conservation after a nonadiabatic transition between vibronic states. When the kinetic energy of the classical subsystem is not sufficient to allow a transition to a higher vibronic state (i.e., a "classically forbidden transition"), the transition is rejected with no adjustment to the velocity.

The MDQT method has been tested by comparison to fully quantum dynamical calculations for model systems. The simplest model PCET system studied includes one electron coordinate, one proton coordinate, and one solvent degree of freedom representing a collective solvent mode without any dissipation.[41] Both MDQT and fully quantum dynamical calculations were propagated for this system. In the MDQT calculations, the proton and electron coordinates were treated quantum mechanically, while the solvent coordinate was treated classically, and the trajectories were propagated on the adiabatic electron−proton vibronic potential energy surfaces. The agreement between the MDQT and fully quantum dynamical calculations provides validation for the application of the MDQT method to these types of systems.[41] In addition, the MDQT method has been applied to a proton transfer reaction represented by a symmetric double well system coupled to a dissipative bath.[53] For this model study, the MDQT results agreed well with numerically exact results[54] in the spatial-diffusion-controlled regime, which is relevant to the present work.[53]

This approach is based on a number of well-defined approximations. The collective solvent coordinate x and the

reorganization energy λ are assumed to be independent of the proton coordinate r_p. This assumption is equivalent to the assumption that the solute−solvent interaction energies for each diabatic electronic state are independent of the proton coordinate.[34] In this case, the free energy and the potential energy along the proton coordinate are equivalent (i.e., the entropic effects are included in the $f_0x^2/2$ term in eq 14 and do not depend on r_p). Thus, the adiabatic electron−proton vibronic free energy surfaces can be generated with the surrogate vibronic Hamiltonian in eq 14, which is defined in terms of free energies rather than potential energies. Furthermore, in this approach, the electron−proton nonadiabatic effects are included in the generation of the electron−proton vibronic free energy surfaces, while the nonadiabatic effects between the electron−proton subsystem and the solvent are included with the MDQT method. The MDQT method can be applied to these free energy surfaces because the entropy is fixed during a nonadiabatic transition, which occurs at a fixed value of the collective solvent coordinate.

III. Model Calculations

A. Model Systems. In this subsection, we define the series of model systems studied in the present paper. For all models studied, the proton potentials corresponding to the donor and acceptor diabatic electronic states $|D\rangle$ and $|A\rangle$ are harmonic with the same frequency ω_p and minima at $r_p = r_p^D$ and $r_p = r_p^A$, respectively

$$U^D(r_p) = \frac{1}{2}m_p\omega_p^2(r_p - r_p^D)^2$$
$$U^A(r_p) = \frac{1}{2}m_p\omega_p^2(r_p - r_p^A)^2 \quad (21)$$

Prior to photoexcitation, the system is in the electronic ground state, where the proton potential is of the form $U^0(r_p) = (1/2)m_p\omega_p^2r_p^2$. The equilibrium distribution of the collective solvent coordinate in the electronic ground state is chosen to be the same as that of the acceptor diabatic electronic state $|A\rangle$.

Photoexcitation from the electronic ground state to the excited donor electronic state $|D\rangle$ is assumed to be instantaneous. As discussed in section II.D, the proton basis functions are chosen to be the harmonic oscillator eigenfunctions associated with the potential energy $U^0(r_p)$. Prior to photoexcitation, the system is assumed to be in the ground proton vibrational state $|\chi_0\rangle$ of the electronic ground state. Thus, the electron−proton wave function following photoexcitation, which is the initial wave function in our calculations, is

$$\Psi(t = 0) = |D\rangle|\chi_0\rangle \quad (22)$$

In addition, the solvent configuration at time $t = 0$ is assumed to correspond to the classical Gaussian distribution associated with the function $(1/2)f_0[x - (2\lambda/f_0)^{1/2}]^2$.

We consider two cases that differ in the relative positions of the minima of the proton potentials in the ground and excited electronic states. In both cases, the proton potentials in the photoexcited donor and acceptor electronic states $|D\rangle$ and $|A\rangle$ are separated by 0.5 Å, and the minimum of the proton potential in the electronic ground state is at $r_p = 0$. In Case I, the proton potential in the electronic ground state is centered at the same position as the proton potential in the photoexcited donor electronic state $|D\rangle$, $r_p^D = 0$ and $r_p^A = 0.5$ Å. In Case II, the proton potential in the electronic ground state is located midway between the proton potentials in the photoexcited donor and acceptor electronic states, $r_p^D = -0.25$ Å and $r_p^A = 0.25$ Å. For Case I, $U^D(r_p)$ and $U^0(r_p)$ are centered at the same value of the proton coordinate, and the proton wavepacket at $t = 0$ is the ground proton vibrational state in the donor electronic state $|D\rangle$. For Case II, $U^D(r_p)$ is shifted with respect to $U^0(r_p)$, and the proton wavepacket at $t = 0$ is a coherent mixture of several proton vibrational states in the donor electronic state, with weightings determined by the Franck−Condon overlaps between $|\chi_0\rangle$ and the proton vibrational wave functions corresponding to $U^D(r_p)$.

The physical characteristics of these models are illustrated schematically in Figure 1. Figure 1a depicts the proton potentials in the electronic ground state and the photoexcited donor and

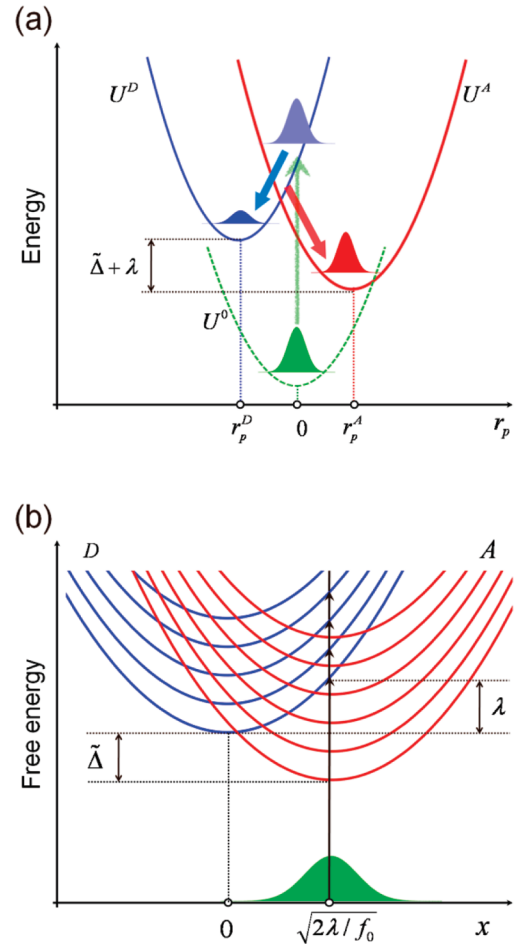

Figure 1. Schematic picture of the model photoinduced PCET system. (a) Proton potentials as functions of the proton coordinate. The proton potential $U^0(r_p)$ corresponds to the electronic ground state prior to photoexcitation. The proton potentials $U^D(r_p)$ and $U^A(r_p)$ correspond to the photoexcited donor and acceptor electronic states $|D\rangle$ and $|A\rangle$, respectively. The energy difference between the minima of $U^D(r_p)$ and $U^A(r_p)$ is $\lambda + \tilde{\Delta}$ because the potentials are calculated from the diagonal elements of H^{vib} in eq 14 evaluated at $x = x_A$, the equilibrium collective solvent coordinate for the acceptor state $|A\rangle$. (b) Diabatic electron−proton vibronic free energy surfaces as functions of the collective solvent coordinate. The donor vibronic states are in blue, and the acceptor vibronic states are in red. These surfaces can be obtained by diagonalizing the donor and acceptor blocks of H^{vib} in eq 14 in an electron−proton vibronic basis. The donor and acceptor vibronic surfaces are parabolic with minima at $x_D = 0$ and $x_A = (2\lambda/f_0)^{1/2}$, respectively. The initial Gaussian distribution of the collective solvent coordinate, which is centered at $x = x_A$, is depicted in green, and the photoexcitation of this distribution to the donor vibronic states is illustrated by black arrows. The reorganization energy λ and the energy bias $\tilde{\Delta}$ are also indicated.

TABLE 1: Parameters Used in the Model Studies for Water and Methanol

parameter	water	methanol
T (K)	298	293
ε_0	79.2[a]	33.7[c]
ε_∞	4.2[a]	5.6[c]
f_0	55.7	84.4
τ_D (ps)	8.72[a]	55.6[c]
τ_L (ps)	0.462	9.24
I (kg m^2)[e]	1.96×10^{-47} [b]	2.53×10^{-46} [d]
ω_{rot} (ps^{-1})	14.5	4.00
τ_O (ps)	0.01030	0.006777
m_x (ps^2)	0.265	5.28
λ (eV)	0.65	0.65
$(2\lambda/f_0)^{1/2}$ (eV$^{1/2}$)	0.153	0.124

[a] Values from ref 69. [b] Value from ref 70. [c] Values from ref 71. [d] Value from ref 72. [e] $I = (I_{xx} + I_{yy} + I_{zz})/3$.

acceptor electronic states $|D\rangle$ and $|A\rangle$. The curves labeled as $U^D(r_p)$ and $U^A(r_p)$ correspond to the diagonal elements of H^{vib} in eq 14 evaluated at $x = (2\lambda/f_0)^{1/2}$ (i.e., at the equilibrium collective solvent coordinate for the acceptor state $|A\rangle$). Thus, the energy difference between the minima of $U^D(r_p)$ and $U^A(r_p)$ is $\lambda + \tilde{\Delta}$. This figure corresponds to Case II, in which the proton potential $U^0(r_p)$ is centered at the midpoint between the donor and acceptor proton potentials.

Figure 1b depicts the diabatic electron−proton vibronic free energy surfaces as functions of the collective solvent coordinate x for the donor and acceptor states $|D\rangle$ and $|A\rangle$. These surfaces can be obtained by diagonalization of the donor and acceptor blocks of the surrogate vibronic Hamiltonian in eq 14 in the electron−proton vibronic basis described in section II.D. The donor and acceptor diabatic vibronic surfaces are parabolic with minima at $x_D = 0$ and $x_A = (2\lambda/f_0)^{1/2}$, respectively. In this paper, the terms donor and acceptor will always refer to diabatic states or surfaces. The initial Gaussian distribution of the collective solvent coordinate, which is centered at $x = x_A$, and the photoexcitation to the donor vibronic states are also shown. For Case I, the system is photoexcited into the lowest-energy donor vibronic state (i.e., the lowest-energy blue parabola in Figure 1b). For Case II, the system is photoexcited into a coherent mixture of donor vibronic states (i.e, a mixture of several blue parabolas in Figure 1b), with the initial population of each donor vibronic state determined by the Franck−Condon factors.

Within these two cases, we consider three models with different energy biases between the donor and acceptor states, $\tilde{\Delta} = 0$, 1.0, and 3.51 eV, which are denoted models A, B, and C, respectively. The electronic coupling is $V_{DA} = 0.03$ eV, and the proton frequency is $\omega_p = 3000$ cm^{-1} in all models. We also study the solvent effects on the nonadiabatic dynamics by performing the calculations for both water and methanol. In our approach, the input quantities that characterize the solvent are the inertial and optical dielectric constants, ε_0 and ε_∞, the Debye relaxation time τ_D, the moment of inertia I of an individual solvent molecule, and the solvent reorganization energy λ. The solvent parameters for water and methanol are given in Table 1. To focus on the difference in solvent relaxation times, we use the same solvent reorganization energy and energy biases for both solvents, although these parameters will also differ for the two solvents. Note that $x_A = 0.153$ (eV)$^{1/2}$ for water and 0.124 (eV)$^{1/2}$ for methanol.

These models provide a reasonable description of the two types of chemical processes given in eqs 1 and 2, which correspond to photoinduced PCET in charge transfer excited states of hydrogen-bonded organic molecules and quenching of MLCT excited states in transition metal complexes, respectively.[14] For these processes, the proton potentials $U^0(r_p)$ and $U^D(r_p)$ are similar because the proton is bonded to the same atom, while the proton potential $U^A(r_p)$ is shifted relative to the other two proton potentials because the proton has transferred and is bonded to a different atom. Thus, these processes correspond to Case I, where the proton potential $U^0(r_p)$ is centered directly below $U^D(r_p)$. For the process given in eq 1, the proton potential $U^D(r_p)$ may be shifted slightly relative to $U^0(r_p)$ due to stretching of the O−H bond, but this shift is expected to be in the opposite direction as that shown in Figure 1a. Note that only the magnitude of the shift between $U^0(r_p)$ and $U^D(r_p)$ impacts the initial populations of the donor vibronic states following photoexcitation, and the direction of the shift does not affect the overall dynamics.

For both processes given in eqs 1 and 2, the equilibrium solvent configuration is distinctly different for the donor and acceptor states due to differences in electronic charge distribution, but the equilibrium solvent configuration for the electronic ground state is similar to that of the acceptor state. Thus, these processes are consistent with the situation depicted in Figure 1b, where the donor and acceptor states are associated with different equilibrium collective solvent coordinates (i.e., the blue and red parabolas have different minima). Moreover, the initial Gaussian distribution of the collective solvent coordinate (shown in green) corresponds to the equilibrium solvent configuration for the acceptor state. Note that the energy bias between the donor and acceptor states, as well as the properties of the hydrogen-bonding interface, can be modified experimentally through the use of substituents that alter the redox potentials and pK_a values of the molecules.

B. Simulation Details. The MDQT method requires the propagation of an ensemble of molecular dynamics trajectories. For each model studied, we propagated 1000 trajectories, although the population decay times were converged with ∼200 trajectories. The initial value of the collective solvent coordinate and the initial donor vibronic state were chosen from distributions corresponding to the initial conditions described above. The initial velocity of the collective solvent coordinate was chosen from a Maxwell−Boltzmann distribution corresponding to the specified temperature. The classical equations of motion were integrated using the velocity Verlet algorithm adapted for Langevin dynamics.[55,56] The time step was 1 atomic unit of time (∼0.024 fs). The time-dependent Schrödinger equation was integrated using the fourth-order Runge−Kutta method[57] with a time step of 0.1 atomic unit of time.

The MDQT trajectories were propagated on the adiabatic vibronic surfaces, as indicated by previous tests of surface hopping methods.[58,59] The adiabatic vibronic states were obtained by full diagonalization of the surrogate vibronic Hamiltonian in eq 14 in an electron−proton basis. For an ensemble of trajectories, this method provides the populations of the adiabatic vibronic states as a function of time. We confirmed that the equilibrium Boltzmann populations among the adiabatic vibronic states are obtained after a sufficient time period. From a physical standpoint, however, the EPT reaction is more easily interpreted in terms of transitions between the donor and acceptor diabatic vibronic states, which correspond to the electron localized on the donor or the acceptor. As mentioned above, the donor and acceptor diabatic vibronic states (i.e., the vibronic states associated with the diabatic electronic states $|D\rangle$ and $|A\rangle$, respectively) are obtained by diagonalizing the respective blocks of this matrix. Unfortunately, conversion between the adiabatic and diabatic vibronic states relies upon the

coherences, which are not well-defined in the MDQT method because the classically forbidden transitions lead to discrepancies between the populations of the states and the quantum probabilities obtained from the quantum amplitudes.[58,60]

For these model systems, which are characterized by relatively small vibronic coupling, the adiabatic and diabatic vibronic states are nearly identical everywhere except in the vicinity of an avoided crossing. Thus, each adiabatic vibronic state can be associated with a diabatic vibronic state for virtually all values of the collective solvent coordinate. In practice, we used the following procedure to obtain the total donor and acceptor state populations as a function of time. At any given time, a MDQT trajectory is in a specified adiabatic state, which is expressed as a linear combination of the $2n_p$ electron−proton vibronic basis functions defined in eq 17. We summed the squares of the coefficients of the basis functions within each block corresponding to the donor state $|D\rangle$ and the acceptor state $|A\rangle$ and selected the block with the larger value. Thus, at every time step in each trajectory, the system was assigned to either the donor or the acceptor state, and the total donor and acceptor state populations were obtained by averaging over an ensemble of MDQT trajectories.

We converged the results with respect to the number of proton vibrational basis functions included in the electron−proton basis. We used 30, 40, 55, 30, 30, and 40 proton vibrational states for Models IA, IB, IC, IIA, IIB, and IIC, respectively. Note that the conversion between adiabatic and diabatic states is straightforward at time $t = 0$ because the coherences are known. Thus, the initial populations of the adiabatic vibronic states are determined by expressing the diabatic wave function in eq 22 as a linear combination of adiabatic vibronic states.

C. Case I Models. In Case I, the proton potential in the electronic ground state is centered at the same position as the proton potential in the photoexcited donor state $|D\rangle$. In this case, the initial proton wavepacket immediately following photoexcitation is in the ground vibrational state of the diabatic electronic state $|D\rangle$ (i.e., the lowest-energy donor state). As discussed above, the MDQT trajectories are propagated on the adiabatic vibronic free energy surfaces. Figure 2 depicts the adiabatic vibronic surfaces as functions of the collective solvent coordinate with water as the solvent for three different energy biases. The correspondence between the adiabatic and diabatic vibronic surfaces is clear from this figure, where the minima of the donor and acceptor diabatic vibronic surfaces are at $x = x_D$ and x_A, respectively. Initially the solvent coordinate is a Gaussian distribution centered at $x = x_A$.

1. Model IA. Figures 3a and 2d depict the adiabatic vibronic state populations and the solvent coordinate distribution as functions of time for the Case I model with no energy bias in water. Figure 3b depicts the fraction of trajectories with the solvent coordinate closer to either $x = x_D$ (blue) or x_A (red) as a function of time for this model. Initially, the second, third, and fourth adiabatic vibronic states are occupied, and the solvent distribution is centered at $x = x_A$. The system relaxes to the ground adiabatic vibronic state, and the solvent distribution shifts to be centered at $x = x_D$ in less than 1 ps. As shown in Figure 3c, which depicts the donor and acceptor state populations, the total population of the donor state remains unity on this time scale of the solvent relaxation. Thus, no EPT occurs during this time period.

The arrow in Figure 2a illustrates this mechanism, which involves fast solvent relaxation without EPT. Figure 4a depicts a specific trajectory that starts in the third adiabatic vibronic state (brown) and makes a nonadiabatic transition to the second adiabatic vibronic state (green) due to strong nonadiabatic coupling, as manifested by the small splitting between the adiabatic vibronic surfaces. Physically, this process corresponds to remaining in the donor state. Note that eventually, the system will reach equilibrium, with equal populations in the donor and acceptor states. In this model, however, the time scale of the solvent dynamics is much faster than that of the electron−proton dynamics, and the EPT rate is independent of the solvent relaxation time scale.

The adiabatic state populations with methanol as the solvent are shown in Figure 3d. A comparison of Figures 3a and d indicates that the qualitative behavior in methanol is similar to that observed in water, except the relaxation process is approximately 20 times slower in methanol. This slower relaxation time scale in methanol is expected since the longitudinal relaxation time τ_L is 20 times greater for methanol than for water. These calculations provide confirmation that the initial relaxation time is dictated solely by the solvent dynamics.

2. Model IB. Figures 5a and 2e depict the adiabatic vibronic state populations and the solvent coordinate distribution as functions of time for the Case I model with a 1.0 eV energy bias in water. Figure 5b depicts the fraction of trajectories with the solvent coordinate closer to either $x = x_D$ (blue) or x_A (red) as a function of time for this model. Initially the fifth, sixth, and seventh adiabatic vibronic states are occupied, and the solvent distribution is centered at $x = x_A$. The system relaxes to the second, third, and fourth adiabatic vibronic states, and the solvent distribution shifts closer to $x = x_D$ within 1 ps. Subsequently, the system continues to relax predominantly to the second and third adiabatic vibronic state in ~25 ps. During this time period, the solvent distribution bifurcates, and by 50 ps, the distribution is centered at $x = x_A$. Since our model does not include a mechanism for direct vibrational relaxation within a diabatic electronic state, the system remains in the second and third adiabatic vibronic states.

The total donor and acceptor state populations are shown in Figure 5c. With this energy bias, the EPT is much faster than that in Model IA, and most of the population is in the acceptor state after 50 ps. The diabatic state populations with methanol as the solvent are shown in Figure 5d. The overall rate of EPT is approximately two times faster in water than in methanol, indicating that the EPT dynamics is partially controlled by the solvent dynamics.

The arrows in Figure 2b illustrate the dominant mechanism for this model system. Initially, there is a fast decay (1 ps time scale) of the type observed for Model IA, where the trajectories remain on the lowest-energy donor vibronic surface and slide down toward $x = x_D$. Unlike Model IA, however, the trajectories do not become stuck in the lowest-energy donor vibronic state because several channels to acceptor vibronic states are energetically accessible. Subsequently, the trajectories evolve predominantly on the second and third adiabatic vibronic surfaces, sometimes (but not always) making nonadiabatic transitions between adiabatic vibronic states. After approximately 50 ps, the majority of the population ends up in the second adiabatic vibronic state with the solvent distribution centered at $x = x_A$. Physically, this situation corresponds to moving in the donor state, with part of the population switching to the acceptor state at each crossing until most of the population ends up in the acceptor state.

3. Model IC. Figures 6a and 2f depict the adiabatic vibronic state populations and the solvent coordinate distribution as functions of time for the Case I model with a 3.51 eV energy bias in water. Figure 6b depicts the fraction of trajectories with

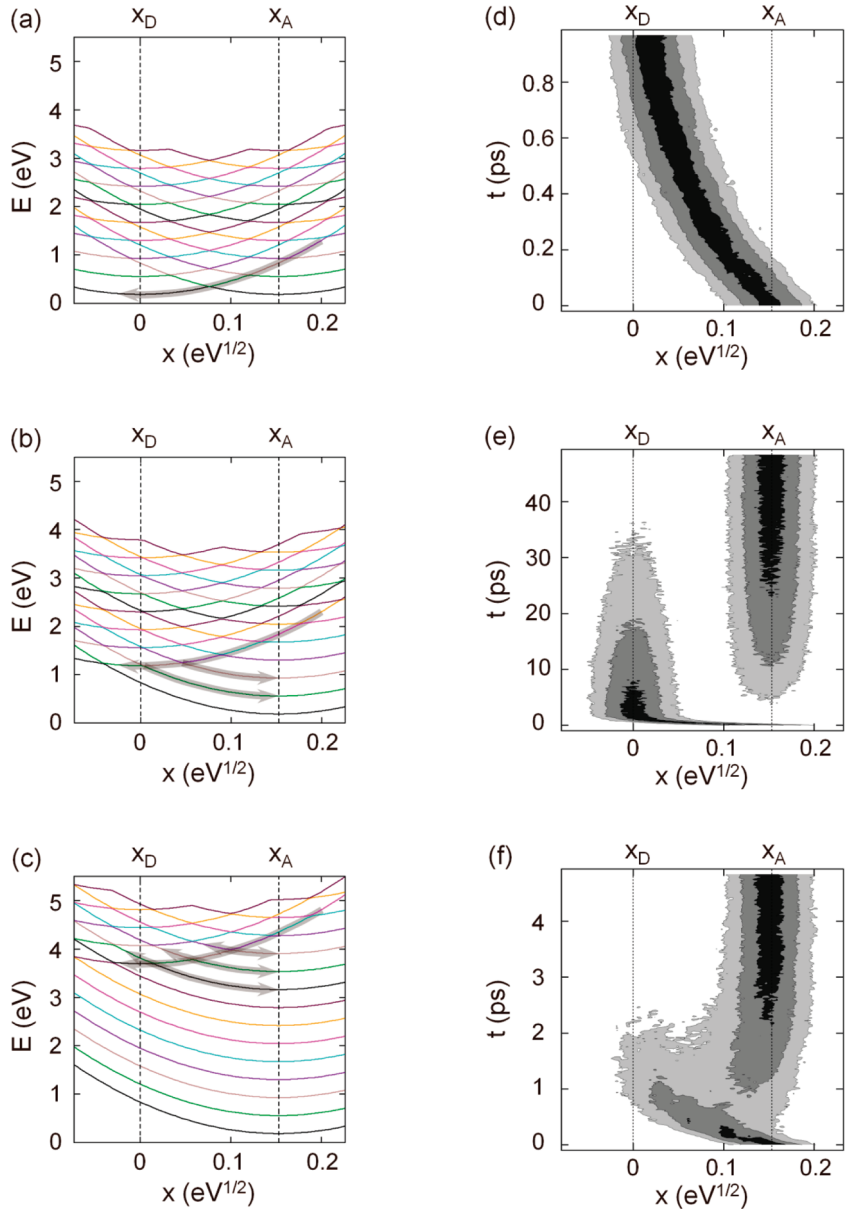

Figure 2. Adiabatic vibronic free energy surfaces as functions of the collective solvent coordinate (left) and time dependence of the solvent coordinate distribution (right) for the Case I model systems in water. The results are shown for models with zero energy bias in (a) and (d), 1.0 eV energy bias in (b) and (e), and 3.51 eV energy bias in (c) and (f). On the left, each adiabatic vibronic surface is given a unique color (i.e., the ground adiabatic vibronic state is black). The donor and acceptor vibronic surfaces are evident as parabolas with minima at $x = x_D$ and x_A, respectively. All trajectories start in the lowest-energy donor vibronic state, and the gray arrows indicate the dominant pathways for the trajectories. On the right, the solvent coordinate distribution is illustrated by a contour plot where the darker color indicates greater probability. In (a), most trajectories remain on the lowest-energy donor vibronic state and end up with $x \approx x_D$ in the ground adiabatic vibronic state (black curve) in ~1 ps. EPT is not observed on this time scale, and the observed relaxation time is determined entirely by the solvent dynamics. In (b), most trajectories remain on the lowest-energy donor vibronic state for the first 1 ps but then continue to move predominantly on the second and third adiabatic vibronic surfaces for ~50 ps, switching between the donor and acceptor vibronic states, until the majority of trajectories end up with $x \approx x_A$ in the second adiabatic vibronic state (green curve). EPT occurs on a slightly longer time scale than the solvent dynamics, but these processes are coupled. In (c), most trajectories start in the 12th and 13th adiabatic vibronic states, quickly relax down to the 9th−11th adiabatic vibronic states, and move dynamically on these surfaces for ~3 ps, switching between the donor and acceptor vibronic states, until most trajectories end up with $x \approx x_A$ in the 9th through 11th adiabatic vibronic states. EPT occurs on a similar time scale as the solvent dynamics, and these processes are strongly coupled.

the solvent coordinate closer to either $x = x_D$ (blue) or x_A (red) as a function of time for this model. Initially the 12th, 13th, and 14th adiabatic vibronic states are occupied, and the solvent distribution is centered at $x = x_A$. The system relaxes to the 9th, 10th, and 11th adiabatic vibronic states, and the solvent distribution shifts toward $x = x_D$ within 1 ps. The populations of the adiabatic vibronic states stabilize, and the solvent distribution becomes centered at $x = x_A$ again within 3 ps. As shown by Figure 6c, which depicts the donor and acceptor state populations, the EPT is nearly complete within 3 ps. In this case, the EPT is much faster than that in the previous models and is on a similar time scale as the solvent relaxation dynamics. Figure 6d depicts the donor and acceptor state populations for this model in methanol. The EPT is approximately 10 times slower in methanol than in water. For this model, the EPT dynamics is even more strongly coupled to the solvent dynamics than that in Model IB, and the overall rate is significantly influenced by the solvent relaxation time scale.

The arrows in Figure 2c illustrate this mechanism, which involves fast, strongly coupled solvent dynamics and EPT.

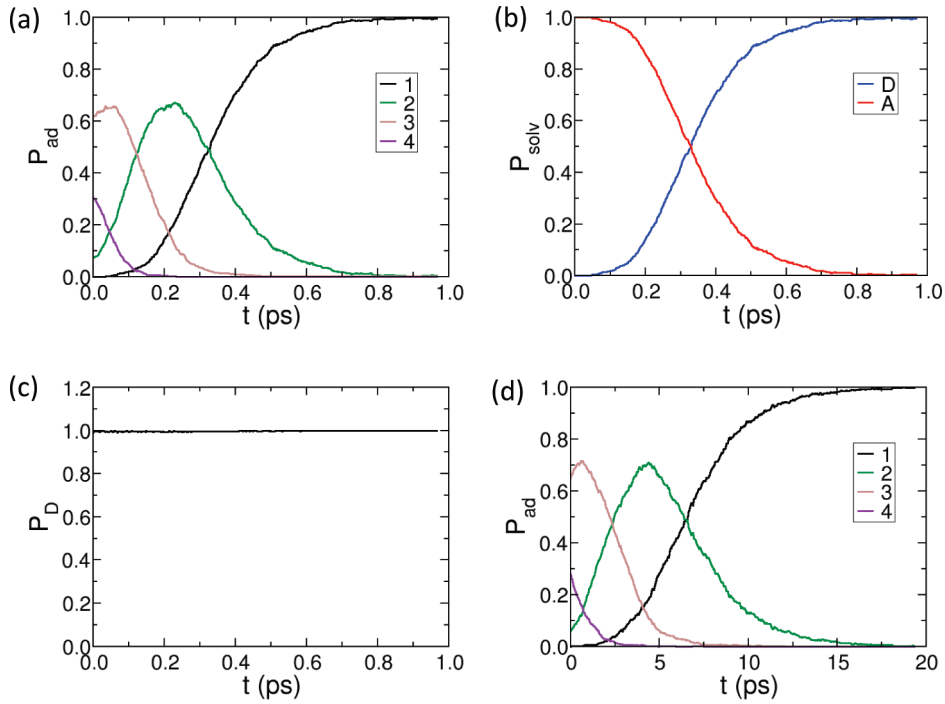

Figure 3. Results from MDQT calculations for the PCET model system corresponding to Case I with no energy bias (Model IA). (a) Populations of adiabatic vibronic states as functions of time for the model in water. (b) Fraction of trajectories with the solvent coordinate closer to either $x = x_D$ (blue) or x_A (red) as a function of time for the model in water. (c) Population of donor state as a function of time for the model in water. Note that the entire population remains in the donor state for this model on this time scale. (d) Populations of adiabatic vibronic states as functions of time for the model in methanol.

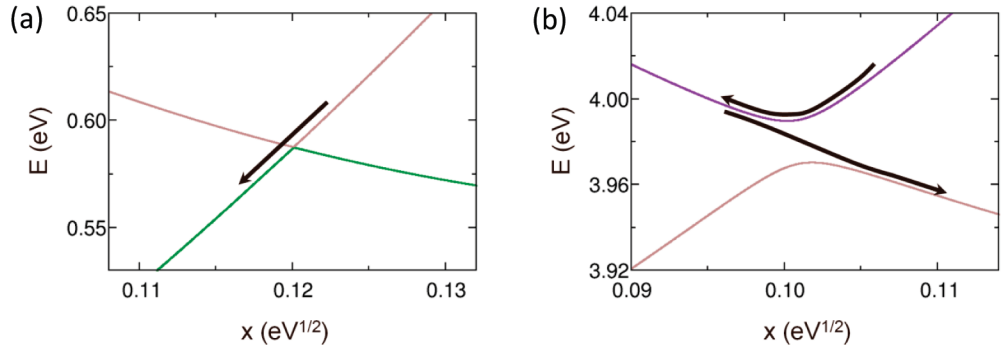

Figure 4. Avoided crossing between the (a) 2nd and 3rd adiabatic vibronic states for Model IA and (b) 11th and 12th adiabatic vibronic states for Model IC. The pathway of a representative trajectory is depicted with a black arrow. In (a), the splitting between adiabatic vibronic states is small, so the trajectory makes a nonadiabatic transition between the adiabatic states, thereby remaining in the donor state. In (b), the splitting between adiabatic vibronic states is large, so the trajectory does not make a nonadiabatic transition between the adiabatic states in the first passing but does make a nonadiabatic transition between the adiabatic states in the second passing, thereby ending up in the acceptor state.

Figure 4b depicts a trajectory that starts in the 12th adiabatic vibronic state (purple) and remains in this adiabatic vibronic state through the avoided crossing due to small nonadiabatic coupling, as manifested by the large splitting between the adiabatic vibronic states. Subsequently, the trajectory reverses direction and makes a nonadiabatic transition down to the 11th adiabatic vibronic state (brown) on the return crossing. Physically, this process corresponds to switching from the donor state to the acceptor state on the first pass through the crossing, which represents EPT, followed by solvent relaxation on the acceptor state. Other trajectories may involve multiple passes through the crossing region, with nonadiabatic transitions on either side of the crossing, leading to the many possible pathways shown in Figure 2c. The overall process, which involves a combination of EPT and solvent dynamics, is completed in ~3 ps.

4. Analysis of Differences among Case I Models. The differences in the dynamical behavior among Models IA, IB, and IC are due primarily to the differences in the vibronic couplings between the relevant donor and acceptor vibronic states. In our models, the vibronic coupling between a pair of donor and acceptor vibronic states is the product of the constant electronic coupling V_{DA} and the overlap integral between the corresponding donor and acceptor proton vibrational wave functions. The donor and acceptor proton vibrational wave functions are the eigenfunctions associated with the harmonic potentials $U^D(r_p)$ and $U^A(r_p)$, respectively.

The splitting between the adiabatic vibronic states at an avoided crossing is approximately two times the vibronic coupling between the corresponding pair of intersecting donor/acceptor diabatic vibronic states. Figure 4a depicts the avoided crossing between the 2nd and 3rd adiabatic vibronic states, and Figure 4b depicts the avoided crossing between the 11th and 12th adiabatic vibronic states. The energy splitting between the adiabatic vibronic states is significantly larger for the latter than for the former. As discussed above and illustrated by the arrows

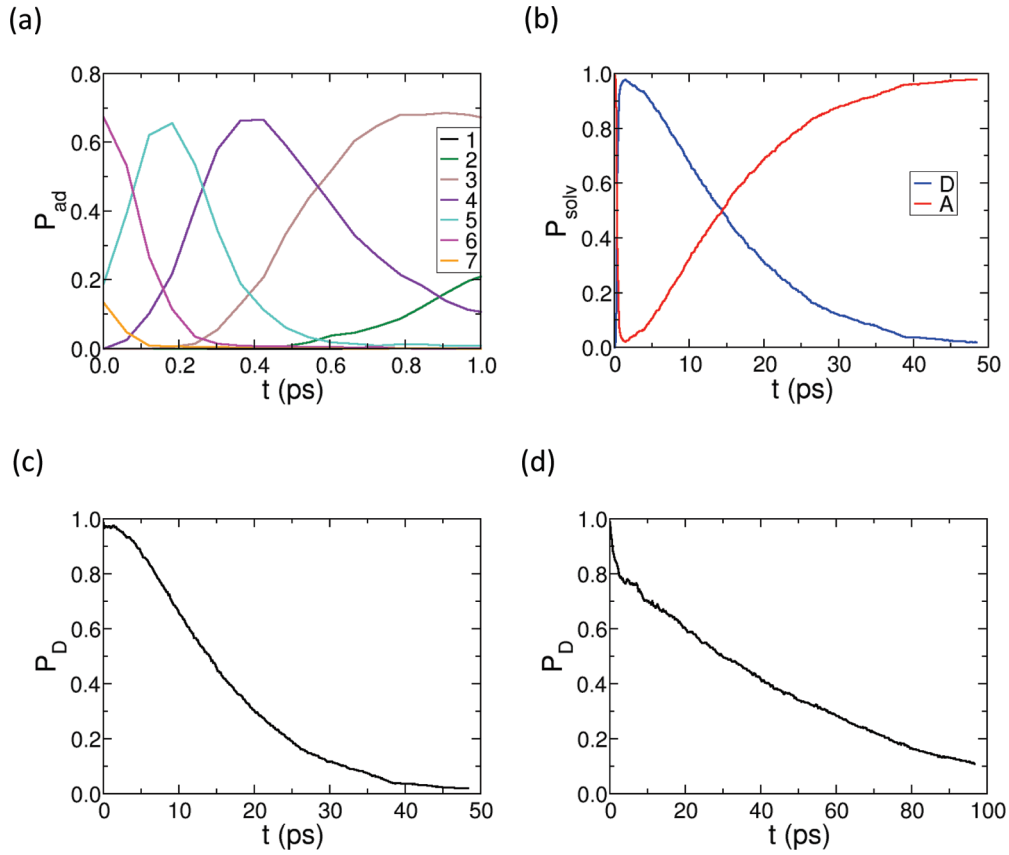

Figure 5. Results from MDQT calculations for the PCET model system corresponding to Case I with 1.0 eV energy bias (Model IB). (a) Populations of adiabatic vibronic states as functions of time for the model in water for the initial 1 ps. When this plot is extended to a longer time scale, the populations of the second and third states cross at ~2 ps, and at 50 ps, the populations of the second and third adiabatic vibronic states are 0.85 and 0.13, respectively. (b) Fraction of trajectories with the solvent coordinate closer to either $x = x_D$ (blue) or x_A (red) as a function of time for the model in water. (c) Population of the donor state as a function of time for the model in water. (d) Population of the donor state as a function of time for the model in methanol.

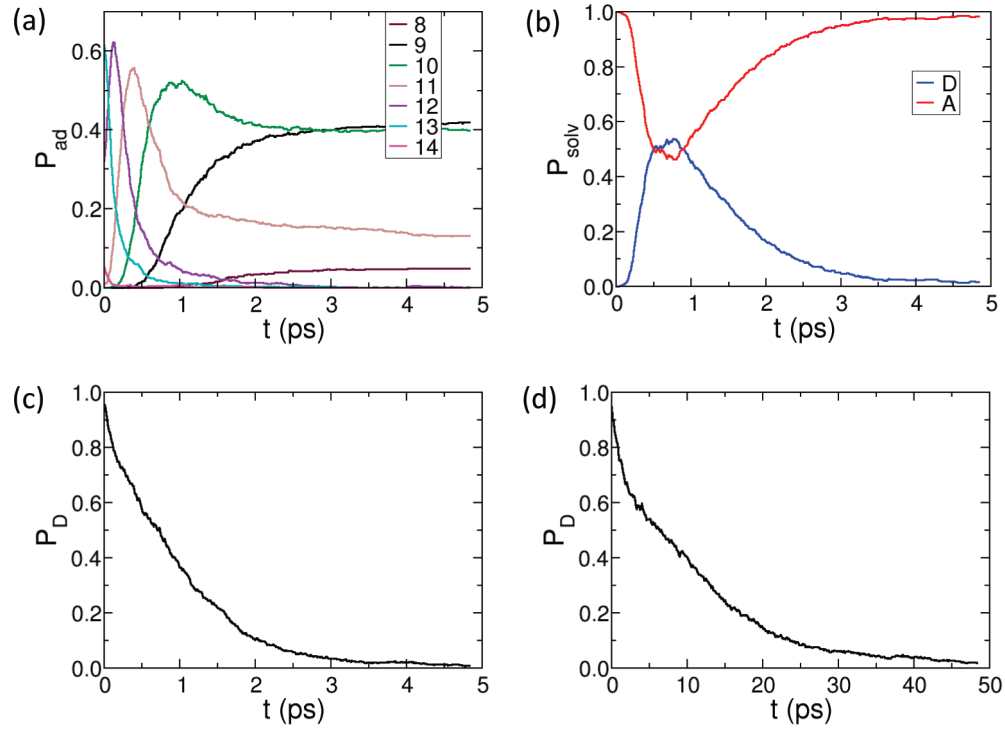

Figure 6. Results from MDQT calculations for the PCET model system corresponding to Case I with 3.51 eV energy bias (Model IC). (a) Populations of adiabatic vibronic states as functions of time for the model in water. (b) Fraction of trajectories with the solvent coordinate closer to either $x = x_D$ (blue) or x_A (red) as a function of time for the model in water. (c) Population of the donor state as a function of time for the model in water. (d) Population of the donor state as a function of time for the model in methanol.

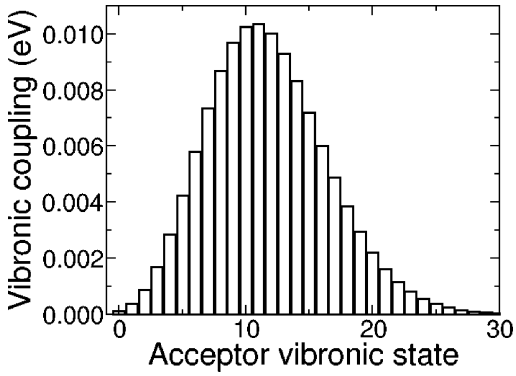

Figure 7. Vibronic coupling between the lowest-energy donor vibronic state and an acceptor vibronic state as a function of the quantum number of the acceptor vibronic state.

in Figure 4, the dynamical behavior of trajectories is very different for these two types of avoided crossings.

The physical basis for the difference in the energy splittings manifested in Figure 4 is illustrated by Figure 7. This figure depicts the vibronic coupling between the lowest-energy donor vibronic state and an acceptor vibronic state as a function of the quantum number of the acceptor vibronic state. As mentioned above, the vibronic coupling is the product of the constant electronic coupling V_{DA} and the overlap integral between the donor and acceptor proton vibrational wave functions. Initially, the vibronic coupling increases as the quantum number of the acceptor state increases because the overlap integral is dominated by the tails of the vibrational wave functions, and the excited proton vibrational wave functions become progressively more delocalized. For highly excited acceptor vibrational states, however, the overlap integral starts to decrease because oscillations of the proton vibrational wave functions lead to cancellation effects. Figure 4a depicts an avoided crossing for lower adiabatic vibronic states, which are associated with a very small overlap integral and therefore small vibronic coupling and energy splitting. Figure 4b depicts an avoided crossing for higher adiabatic vibronic states, which are associated with a relatively large overlap integral and therefore larger vibronic coupling and energy splitting.

In all three Case I models, the trajectories start on the lowest-energy donor vibronic state with the solvent distribution centered at $x = x_A$ following photoexcitation. The energy bias between the donor and acceptor electronic states determines the initial populations of the adiabatic vibronic states. As illustrated by Figure 2, the trajectories start on the lower adiabatic vibronic states in Model IA but start on much higher adiabatic vibronic states in Model IC. This difference in the initial populations of the adiabatic vibronic states accounts for the different dynamical behavior. Specifically, the trajectories in Model IA move through avoided crossings of the type depicted in Figure 4a, while the trajectories in Model IC move through avoided crossings of the type depicted in Figure 4b. Model IB is in the intermediate regime.

D. Case II Models. The Case II model systems differ from the Case I model systems in that the proton wavepacket following photoexcitation is shifted relative to the donor proton potential, as depicted in Figure 1a. In this case, the trajectories do not all start in the lowest-energy donor vibronic state but rather start in a coherent mixture of the donor vibronic states that is determined by the Franck−Condon factors. As a result, the analysis is more difficult, particularly in the context of the adiabatic vibronic states. Therefore, we provide only a brief analysis that summarizes the salient points.

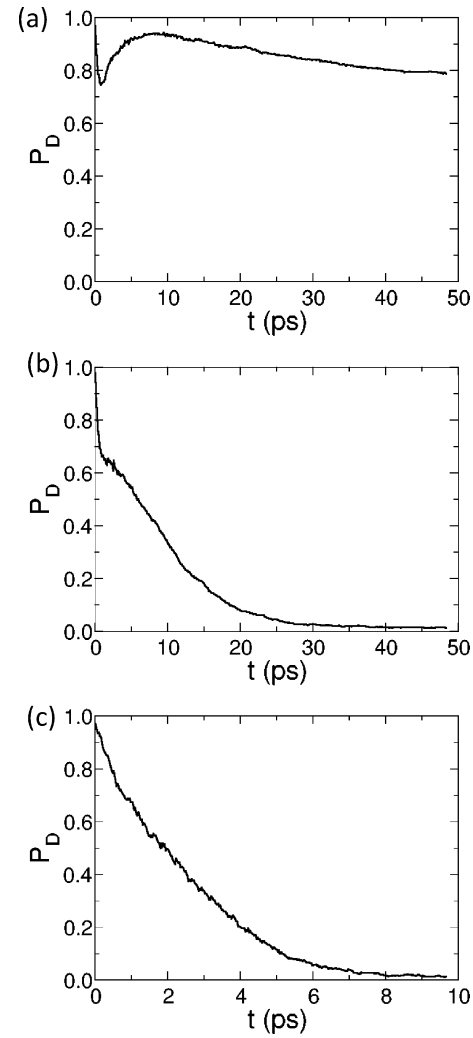

Figure 8. Population of the donor state as a function of time for the PCET model systems corresponding to Case II in water with (a) 0 energy bias (Model IIA), (b) 1.0 eV energy bias (Model IIB), and (c) 3.51 eV energy bias (Model IIC).

Figure 8 depicts the total donor and acceptor state populations as functions of time for Models IIA, IIB, and IIC. These plots are qualitatively similar to the Case I counterparts given in Figures 3c, 5c, and 6c but exhibit some minor differences. In contrast to Model IA, Model IIA exhibits a small amount of EPT, leading to a ∼20% population in the acceptor state after 50 ps. The EPT rate is slightly faster for Model IIB than for Model IB and is slightly slower for Model IIC than for Model IC. These differences arise from the different starting conditions for the trajectories. The underlying physical principles discussed in the previous subsection still govern the qualitative behavior of these model systems.

E. Limitations of Models. In this subsection, we point out the known limitations of these models. One limitation is that the models do not include direct coupling between the proton and the solvent, although the proton is indirectly coupled to the solvent through coupling to the electronic states, which are coupled to the solvent. As a result, proton vibrational relaxation cannot occur by a direct mechanism (i.e., within the donor or acceptor diabatic state) but can occur by an indirect mechanism via nonadiabatic transitions between the donor and acceptor states.[42] We assume that proton vibrational relaxation occurs on a faster time scale for the indirect mechanism than for the direct mechanism because the electron transfer is more strongly

coupled to the solvent than the proton transfer. In this case, the neglect of the direct coupling between the proton and the solvent does not significantly impact the ultrafast dynamics. Another limitation of these models is that they do not include the effects of intramolecular solute modes, such as the proton donor−acceptor mode, which strongly impacts the vibronic coupling.[61] In principle, these effects can be included by modifying the form of the model Hamiltonian.

Other limitations of these models require additional effort to address. For example, these models describe only concerted PCET processes, where the electron and proton transfer in a single step without a stable intermediate. The theoretical formulation presented above can be extended to sequential PCET processes using a four-state model and two collective solvent coordinates corresponding to electron and proton transfer, respectively.[33] Finally, the dielectric continuum solvent model does not describe the effects of the intramolecular solvent modes or hydrogen bonding between the solvent and the solute. The investigation of these effects requires molecular dynamics simulations with explicit solvent molecules.

IV. Concluding Remarks

In this paper, we developed a theoretical formulation for modeling photoinduced nonequilibrium PCET reactions in solution. In this formulation, the PCET system is described by donor and acceptor electron−proton vibronic free energy surfaces that depend on a single collective solvent coordinate defined in the framework of dielectric continuum theory. We obtained a generalized Langevin equation of motion for this collective solvent coordinate. The terms in this equation are defined by the solvent properties, such as the dielectric constants, Debye relaxation time, and molecular moment of inertia, as well as the solute properties characterizing the vibronic surfaces. The ultrafast dynamics following photoexcitation is studied by propagating an ensemble of surface hopping trajectories on the adiabatic electron−proton vibronic surfaces, where the collective solvent coordinate evolves according to the classical Langevin equation of motion.

We used this methodology to examine a series of model photoinduced PCET systems. The initial nonequilibrium state of the solvent coordinate distribution and proton wavepacket was prepared by vertical photoexcitation from the ground electronic state to the donor electronic state. For some models, the EPT rate was much slower than the solvent relaxation time scale; therefore, the two processes were completely uncoupled. For other models, the EPT and solvent dynamics occurred on similar time scales, leading to strong coupling between the two processes. In general, the EPT rate is enhanced by increasing the vibronic coupling between the donor and acceptor states, which corresponds to increasing the electronic coupling or the overlap between the donor and acceptor proton vibrational wave functions. The overlap becomes greater as the separation between the minima of the donor and acceptor proton potentials decreases and as higher excited vibronic states become accessible by the initial photoexcitation. The solute and solvent properties can be tuned to control the coupling between the EPT and the solvent dynamics in photoinduced PCET processes.

The present work provides the foundation for expansions in a variety of different directions. The impact of the proton donor−acceptor motion, which strongly influences the vibronic coupling, can be included by modifying the model Hamiltonian.[61] Other solute modes that are coupled to the PCET reaction (i.e., an essential nuclear rearrangement within the solute) may also be included in this treatment. Moreover, the solvent model can be extended to describe solvents characterized by two different relaxation time scales (i.e., heavier alcohols).[62] In addition, the treatment can be extended to describe both sequential and concerted EPT reactions, as well as to include the direct coupling between the proton and solvent, by deriving the Langevin equations of motion for two collective solvent coordinates corresponding to electron and proton transfer, respectively.[33] Furthermore, this formulation can be used to study hydrogen/deuterium isotope effects[42] and can be extended to electrochemical systems.[63−65] Finally, photoinduced PCET reactions can be simulated with all-atom molecular dynamics of explicit solute and solvent molecules described by an ab initio or empirical valence bond potential.

Acknowledgment. We gratefully acknowledge funding from AFOSR Grant FA9550-10-1-0081 and NSF Grant CHE-07-49646.

Appendix

Derivation of the Langevin Equation for the Onodera Model of Dielectric Relaxation. In this Appendix, we derive the Langevin equation based on the Onodera model of dielectric relaxation.[50] In this model, the frequency-dependent dielectric function has the following simple form

$$\varepsilon(\omega) = \varepsilon_\infty + \frac{\varepsilon_0 - \varepsilon_\infty}{(1 - i\omega\tau_D)(1 - i\omega\tau_O)} = \varepsilon'(\omega) + i\varepsilon''(\omega) \tag{A1}$$

where τ_D is the Debye relaxation time and τ_O is an additional parameter related to the characteristic rotational time scale of the solvent molecules. The real and imaginary parts of the dielectric function given in eq A1 satisfy the Kramers−Krönig relationships for generalized susceptibilities

$$\begin{aligned} \varepsilon'(\omega) &= \varepsilon_\infty + \frac{1}{\pi}\mathscr{P}\int_{-\infty}^{\infty} \frac{\varepsilon''(\Omega)}{\Omega - \omega}\, d\Omega \\ \varepsilon''(\omega) &= -\frac{1}{\pi}\mathscr{P}\int_{-\infty}^{\infty} \frac{\varepsilon'(\Omega) - \varepsilon_\infty}{\Omega - \omega}\, d\Omega \end{aligned} \tag{A2}$$

where the symbol $\mathscr{P}$ denotes the Cauchy principal value.

We now turn to the evaluation of the causal dynamical operator $\hat{f}$ entering the equation of motion for the solvent coordinate x given in eq 10. The frequency-dependent factor $f(\omega)$ corresponding to the dielectric function in eq A1 can be easily calculated

$$f(\omega) = \frac{4\pi\varepsilon(\omega)\varepsilon_\infty}{\varepsilon(\omega) - \varepsilon_\infty} = f_0(1 - i\omega\tilde{\tau}_L - \omega^2\tau_O\tau_L) \tag{A3}$$

Here, $f_0 = 4\pi\varepsilon_0\varepsilon_\infty/(\varepsilon_0 - \varepsilon_\infty)$ is the inverse Pekar factor, $\tau_L = \varepsilon_\infty\tau_D/\varepsilon_0$ is the longitudinal relaxation time, and

$$\tilde{\tau}_L = \varepsilon_\infty(\tau_O + \tau_D)/\varepsilon_0 \tag{A4}$$

The inverse Fourier transform of the function $f(\omega)$, which defines the integral kernel of the operator $\hat{f}$, can be evaluated analytically and is given by the following expression containing the first and second derivatives of the Dirac δ-function

$$f(t) = f_0[\delta(t) - \tilde{\tau}_L\delta'(t) - \tau_O\tau_L\delta''(t)] \quad \text{(A5)}$$

Substituting the above expression into the definition of the dynamical operator given in eq 8 and applying it to eq 10, we obtain the following explicit form of the equation of motion for the solvent coordinate x

$$f_0\tau_O\tau_L\ddot{x} = -f_0\tilde{\tau}_L\dot{x} - \frac{dW_k(x)}{dx} + F(t) \quad \text{(A6)}$$

Using eq 13, we can calculate the time correlation function of the random force $F(t)$

$$\langle F(t)F(t')\rangle = 2k_BTf_0\tilde{\tau}_L\delta(t - t') \quad \text{(A7)}$$

As indicated by eq A6, the equation of motion for the solvent described by the Onodera relaxation model includes the acceleration term with an effective mass

$$m_x = f_0\tau_O\tau_L \quad \text{(A8)}$$

This effective mass depends on the properties of the solvent molecules and can be estimated from the microscopic parameters of the solvent.[66,67] We start from the standard equilibrium relation

$$\frac{m_x\langle\dot{x}^2\rangle}{2} = \frac{k_BT}{2} \quad \text{(A9)}$$

which follows from the energy equipartition principle. The time correlation function of the coordinate x can be expressed in terms of the imaginary part of the generalized susceptibility $\kappa(\omega) = [f(\omega)]^{-1}$

$$\langle x(t)x(t')\rangle = \frac{1}{2\pi}\int_{-\infty}^{\infty}\frac{2k_BT}{\omega}\kappa''(\omega)e^{-i\omega(t-t')}\,d\omega \quad \text{(A10)}$$

The average squared velocity can be calculated by taking the second derivative of this time correlation function

$$\langle\dot{x}^2\rangle = \langle[\dot{x}(0)]^2\rangle = -\lim_{t\to 0}\left[\frac{d^2}{dt^2}\langle x(t)x(0)\rangle\right] = \frac{k_BT}{4\pi^2}\int_{-\infty}^{\infty}\frac{\omega\varepsilon''(\omega)}{|\varepsilon(\omega)|^2}\,d\omega \quad \text{(A11)}$$

Thus, the effective mass of the solvent can be defined as

$$m_x = \frac{k_BT}{\langle\dot{x}^2\rangle} = 4\pi^2\left[\int_{-\infty}^{\infty}\frac{\omega\varepsilon''(\omega)}{|\varepsilon(\omega)|^2}\,d\omega\right]^{-1} \quad \text{(A12)}$$

In the case of finite velocity dispersion (as for the equation of motion with an acceleration term), the integral in the above expression can be evaluated approximately as shown in ref 66. This yields the following expression for the effective mass

$$m_x = \frac{f_0}{\eta\omega_{rot}^2} \quad \text{(A13)}$$

where

$$\eta = \frac{2\varepsilon_0 + \varepsilon_\infty}{3\varepsilon_0 g}$$
$$\omega_{rot}^2 = \frac{k_BT}{I} \quad \text{(A14)}$$

Here, g is the Kirkwood correlation factor,[68] and ω_{rot} is the thermal rotational frequency, which depends on the moment of inertia I of the isolated solvent molecule. Following previous work,[66] we assume that $\eta = 1$. Note that due to our specific choice of the solvent coordinate x, which has units of (energy)$^{1/2}$, the effective solvent mass has units of (time)^2. Finally, comparing eqs A8 and A13, we can express the additional parameter τ_O in the Onodera model in terms of the microscopic parameters of the solvent

$$\tau_O = \frac{1}{\eta\omega_{rot}^2\tau_L} \quad \text{(A15)}$$

References and Notes

(1) Hoganson, C. W.; Lydakis-Simantiris, N.; Tang, X.-S.; Tommos, C.; Warncke, K.; Babcock, G. T.; Diner, B. A.; McCracken, J.; Styring, S. *Photosynth. Res.* **1995**, *46*, 177.

(2) Tommos, C.; Tang, X.-S.; Warncke, K.; Hoganson, C. W.; Styring, S.; McCracken, J.; Diner, B. A.; Babcock, G. T. *J. Am. Chem. Soc.* **1995**, *117*, 10325.

(3) Gratzel, M. *Nature* **2001**, *414*, 338.

(4) Alstrum-Acevedo, J. H.; Brennaman, M. K.; Meyer, T. J. *Inorg. Chem.* **2005**, *44*, 6802.

(5) Sproviero, E. M.; Gascon, J. A.; McEvoy, J. P.; Brudvig, G. W.; Batista, V. S. *Curr. Opin. Struct. Biol.* **2007**, *17*, 173.

(6) Prezhdo, O. V.; Duncan, W. R.; Prezhdo, V. V. *Acc. Chem. Res.* **2008**, *41*, 339.

(7) Magnuson, A.; Anderlund, M.; Johansson, O.; Lindblad, P.; Lomoth, R.; Polivka, T.; Ott, S.; Stensjo, K.; Styring, S.; Sundstrom, V.; Hammarstrom, L. *Acc. Chem. Res.* **2009**, *42*, 1899.

(8) Gust, D.; Moore, T. A.; Moore, A. L. *Acc. Chem. Res.* **2009**, *42*, 1890.

(9) Sjodin, M.; Styring, S.; Akermark, B.; Sun, L.; Hammarstrom, L. *J. Am. Chem. Soc.* **2000**, *122*, 3932.

(10) Sjodin, M.; Ghanem, R.; Polivka, T.; Pan, J.; Styring, S.; Sun, L.; Sundstrom, V.; Hammarstrom, L. *Phys. Chem. Chem. Phys.* **2004**, *6*, 4851.

(11) Reece, S. Y.; Nocera, D. G. *J. Am. Chem. Soc.* **2005**, *127*, 9448.

(12) Irebo, T.; Reece, S. Y.; Sjodin, M.; Nocera, D. G.; Hammarstrom, L. *J. Am. Chem. Soc.* **2007**, *129*, 15462.

(13) Concepcion, J. J.; Brennaman, M. K.; Deyton, J. R.; Lebedeva, N. V.; Forbes, M. D. E.; Papanikolas, J. M.; Meyer, T. J. *J. Am. Chem. Soc.* **2007**, *129*, 6968.

(14) Gagliardi, C. J.; Westlake, B. C.; Papanikolas, J. M.; Kent, C. A.; Paul, J. J.; Meyer, T. J. *Coord. Chem. Rev.* (2010), doi: 10.1016/jccr.2010.03.001.

(15) Barzykin, A. V.; Frantsuzov, P. A.; Seki, K.; Tachiya, M. Solvent Effects in Nonadiabatic Electron Transfer Reactions: Theoretical Aspects. In *Advances in Chemical Physics*; Prigogine, I., Rice, S. A., Eds.; Wiley Interscience: New York, 2002; Vol. 123, p 511.

(16) Cukier, R. I.; Nocera, D. G. *Annu. Rev. Phys. Chem.* **1998**, *49*, 337.

(17) Huynh, M. H.; Meyer, T. J. *Chem. Rev.* **2007**, *107*, 5004.

(18) Mayer, J. M. *Annu. Rev. Phys. Chem.* **2004**, *55*, 363.

(19) Hammes-Schiffer, S.; Soudackov, A. V. *J. Phys. Chem. B* **2008**, *112*, 14108.

(20) Cukier, R. I. *J. Phys. Chem.* **1994**, *98*, 2377.

(21) Cukier, R. I. *J. Phys. Chem.* **1996**, *100*, 15428.

(22) Soudackov, A.; Hammes-Schiffer, S. *J. Chem. Phys.* **2000**, *113*, 2385.

(23) Hammes-Schiffer, S. *Acc. Chem. Res.* **2001**, *34*, 273.

(24) Cukier, R. I. *Biochim. Biophys. Acta* **2004**, *1655*, 37.

(25) Marcus, R. A. *Annu. Rev. Phys. Chem.* **1964**, *15*, 155.
(26) Marcus, R. A.; Sutin, N. *Biochim. Biophys. Acta* **1985**, *811*, 265.
(27) Calef, D. F.; Wolynes, P. G. *J. Phys. Chem.* **1983**, *87*, 3387.
(28) Basilevsky, M. V.; Chudinov, G. E. *Mol. Phys.* **1988**, *65*, 1121.
(29) Kim, H. J.; Hynes, J. T. *J. Chem. Phys.* **1992**, *96*, 5088.
(30) Bianco, R.; Timoneda, J. J.; Hynes, J. T. *J. Phys. Chem.* **1994**, *98*, 12103.
(31) Bianco, R.; Hynes, J. T. *J. Chem. Phys.* **1995**, *102*, 7864.
(32) Basilevsky, M. V.; Chudinov, G. E.; Newton, M. D. *Chem. Phys.* **1994**, *179*, 263.
(33) Soudackov, A.; Hammes-Schiffer, S. *J. Chem. Phys.* **1999**, *111*, 4672.
(34) Kobrak, M. N.; Hammes-Schiffer, S. *J. Phys. Chem. B* **2001**, *105*, 10435.
(35) Hatcher, E.; Soudackov, A.; Hammes-Schiffer, S. *Chem. Phys.* **2005**, *319*, 93.
(36) Hatcher, E.; Soudackov, A.; Hammes-Schiffer, S. *J. Phys. Chem. B* **2005**, *109*, 18565.
(37) Tully, J. C. *J. Chem. Phys.* **1990**, *93*, 1061.
(38) Hammes-Schiffer, S.; Tully, J. C. *J. Chem. Phys.* **1994**, *101*, 4657.
(39) Fang, J.-Y.; Hammes-Schiffer, S. *J. Chem. Phys.* **1997**, *107*, 5727.
(40) Fang, J.-Y.; Hammes-Schiffer, S. *J. Chem. Phys.* **1997**, *106*, 8442.
(41) Fang, J.-Y.; Hammes-Schiffer, S. *J. Chem. Phys.* **1997**, *107*, 8933.
(42) Venkataraman, C.; Soudackov, A. V.; Hammes-Schiffer, S. *J. Chem. Phys.* **2009**, *131*, 154502.
(43) Venkataraman, C.; Soudackov, A. V.; Hammes-Schiffer, S. *J. Phys. Chem. C* **2010**, *114*, 487.
(44) Warshel, A. *Computer Modeling of Chemical Reactions in Enzymes and Solutions*; John Wiley & Sons, Inc.: New York, 1991.
(45) Schmitt, U. W.; Voth, G. A. *J. Phys. Chem. B* **1998**, *102*, 5547.
(46) Felderhof, B. U. *J. Chem. Phys.* **1977**, *67*, 493.
(47) Ovchinnikova, M. Y. *Khim. Fiz.* **1985**, *4*, 3.
(48) Hynes, J. T. *J. Phys. Chem.* **1986**, *90*, 3701.
(49) Zusman, L. D. *Chem. Phys.* **1980**, *49*, 295.
(50) Onodera, Y. *J. Phys. Soc. Jpn.* **1993**, *62*, 4104.
(51) Hazra, A.; Nooijen, M. *Int. J. Quantum Chem.* **2003**, *95*, 643.
(52) Basilevsky, M. V.; Chudinov, G. E. *J. Chem. Phys.* **1995**, *103*, 1470.
(53) Kim, S. Y.; Hammes-Schiffer, S. *J. Chem. Phys.* **2006**, *124*, 244102.
(54) Topaler, M.; Makri, N. *J. Chem. Phys.* **1994**, *101*, 7500.
(55) Izaguirre, J. A. Langevin Stabilisation of Multiscale Mollified Dynamics. In *Multiscale Computational Methods in Chemistry and Physics*; Brandt, A., Binder, K., Bernholc, J., Eds.; IOS Press: Amsterdam, The Netherlands, 2001; Vol. 117, p 34.
(56) Vanden-Eijnden, E.; Ciccotti, G. *Chem. Phys. Lett.* **2006**, *429*, 310.
(57) Press, W. H.; Teukolsky, S. A.; Vetterling, W. T.; Flannery, B. P. *Numerical Recipes in Fortran 77: The Art of Scientific Computing*, 2nd ed.; Cambridge University Press: New York, 1992.
(58) Muller, U.; Stock, G. *J. Chem. Phys.* **1997**, *107*, 6230.
(59) Hack, M. D.; Truhlar, D. G. *J. Phys. Chem. A* **2000**, *104*, 7917.
(60) Schmidt, J. R.; Parandekar, P. V.; Tully, J. C. *J. Chem. Phys.* **2008**, *129*, 044104.
(61) Soudackov, A.; Hatcher, E.; Hammes-Schiffer, S. *J. Chem. Phys.* **2005**, *122*, 014505.
(62) Basilevsky, M. V.; Chudinov, G. E. *Mol. Phys.* **1990**, *71*, 461.
(63) Venkataraman, C.; Soudackov, A. V.; Hammes-Schiffer, S. *J. Phys. Chem. C* **2008**, *112*, 12386.
(64) Navrotskaya, I.; Soudackov, A. V.; Hammes-Schiffer, S. *J. Chem. Phys.* **2008**, *128*, 244712.
(65) Costentin, C. *Chem. Rev.* **2009**, *108*, 2145.
(66) Rips, I.; Jortner, J. *J. Chem. Phys.* **1987**, *87*, 2090.
(67) Basilevsky, M. V.; Soudackov, A. V.; Vener, M. V. *Chem. Phys.* **1995**, *200*, 87.
(68) Frohlich, H. *Theory of dielectrics*; Oxford University Press: New York, 1949.
(69) Jarzeba, W.; Walker, G. C.; Johnson, A. E.; Kathlow, M. A.; Barbara, P. F. *J. Phys. Chem.* **1998**, *92*, 7039.
(70) Eisenberg, D.; Kauzmann, W. *The Structure and Properties of Water*; Oxford Press: London, 1969.
(71) Castner, E. W., Jr.; Maroncelli, M.; Fleming, G. R. *J. Chem. Phys.* **1987**, *86*, 1090.
(72) Kalugin, O. N.; Chaban, V. V.; Kolesnik, Y. V. *Russ. J. Phys. Chem. A* **2006**, *80*, 1273.

JP1051547